Full Paper: We monitor slow mechanical tests of highly oriented, hard-elastic polypropylene by in situ X-ray scattering. For the analysis two-dimensional small-angle X-ray scattering (SAXS) and ultra-small-angle X-ray scattering (USAXS) patterns are combined. Direction of strain is the normal to the crystalline lamellae of the polymer. The scattering patterns are transformed into a representation of nanostructure in real space. This is the multidimensional cord distribution function (CDF). From the CDF topological parameters of the semicrystalline nanostructure are extracted and discussed in conjunction to the mechanical data.

In a continuous-strain experiment we observe fracture of an ensemble of weak lamellae into blocks already at an elongation of 2%. These blocks are completely dissolved during further stretching up to 10% (yield point). At higher elongations we observe continuous transformation from crystalline lamellae into an ensemble of rigid needles with 8 nm thickness. The material breaks, as all the lamellae are consumed.

In a fatigue test a load-reversal experiment is carried out between elongations of 10% and 35%. At the beginning of every straining branch strain-induced crystallization generates extended lamellae until a stress of 20 MPa is reached. Thereafter breakup of the lamellae sets in. In the further course of the straining branch an unclear superposition of various mechanisms is observed (e.g. the melting of weak blocks as well as the strain crystallization of new and strong blocks). In the relaxation branch of each load cycle we first observe fast relaxation-induced melting, which is continuously slowing down.

Time-resolved X-ray scattering of poly(propylene) during mechanical tests reveals complex mechanisms with respect to the semicrystalline nanostructure. Crystallization, rupture of lamellae, and melting of fragments are continuously reshaping the domains of the material.

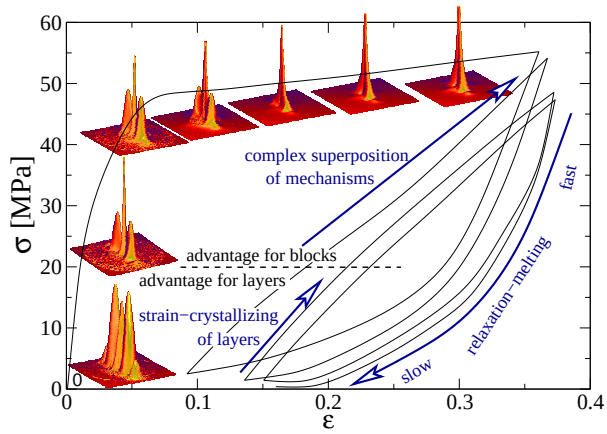

Fatigue test monitored by SAXS. Some scattering patterns and nanostructure evolution mechanisms

Nanostructure Evolution in Polypropylene During Mechanical Testing

Norbert Stribeck[1]*, *Ulrich Nöchel*[1], *Sérgio S. Funari*[2], *Tom Schubert*[2], *Andreas Timmann*[2]

[1]University of Hamburg, Dept. of Chemistry, Institute of Technical and Macromolecular Chemistry, Bundesstr. 45, 20146 Hamburg, Germany. FAX:+49-40-42838-6008; E-mail: Norbert.Stribeck@desy.de
[2]HASYLAB at DESY, 22603 Hamburg, Germany

Keywords: fatigue analysis; mechanical properties; microstructure; poly(propylene) (PP); small-angle X-ray scattering (SAXS)

1 Introduction

The understanding of failure or fatigue mechanisms in polymer materials is of practical relevance, because new lightweight materials with special toughness or low fatigue are urgently sought after. An example is the automotive industry, which needs such materials in order to accomplish the goal of fuel reduction by reduction of weight.

These mechanisms can be studied by methods which provide time-resolved in situ data, like the small-angle X-ray scattering (SAXS). Nevertheless, the available instrumentation is enforcing a compromise. Either low-noise patterns are recorded with poor time resolution, or noisy patterns with good time-resolution are obtained.

For phenomenological surveys it is suitable to relinquish the postulate of recording low-noise scattering patterns using instruments equipped with a very fast detector.[1] In such an environment, structure evolution can be studied at strain rates of $\dot{\varepsilon} \approx 10^{-1}$ s^{-1}, which are common in industrial processes. A selection of corresponding studies[2–5] demonstrates both power and limits of this approach.

Whenever scattering patterns from anisotropic materials shall be evaluated quantitatively, the stretch-hold technique[6] is frequently employed.[7–27] Characteristic of this technique is step-wise elongation and recording of the scattering while the extensometer is idle. As instrumentation technique is advancing, it is now becoming possible to set up a truly dynamic experiment in which low-noise patterns are recorded with a sufficient frame rate, if only the strain rates are kept low ($\dot{\varepsilon} \approx 10^{-3}$ s^{-1}). To our knowledge, the first paper on polymer deformation based on low-noise patterns with an exposure of 15 s and a cycle time of 30 s has been published by

Chen *et al.*[28] In this manner, a stream of high-precision scattering data is obtained. Moreover, this stream can be considered quasi-continuous, if the variation of nanostructure from frame to frame is small. In this case a survey of the mechanisms of structure evolution is becoming possible.

One method of data evaluation starts from nanostructure models. The corresponding scattering patterns are computed and compared to the measured patterns, as has been demonstrated after a continuous-straining experiment of toughened ultra-high molecular-weight polyethylene.[28] Another study[29] presents SAXS data from a fatigue test. An isotropic polyurethane elastomer is subjected to load-reversal cycling, and the shape of the observed ellipsoidal reflection is compared to the model scattering of affinely deformed macrolattices (,[30] chapter 10).

On the other hand, instead of computing a model scattering pattern, it is possible to transform the measured complete[30,31] scattering patterns into a representation of the nanostructure in real space,[32] where structure parameters can be extracted. In this article, the last-mentioned method is demonstrated for polypropylene both after a continuous-straining experiment, and after a fatigue test. We study highly oriented, hard-elastic[33–37] material and strain in the normal direction of the crystalline lamellae. Thus, shear and the formation of micropores[38,39] are prevented[40] for the most part.

Ultimately, we are pursuing this and similar studies in order to identify the mechanisms of nanostructure evolution which are controlling the failure or the fatigue of polymer materials. Such information is required, if a realistic computer model of a polymer material shall be set up in order to predict tailored materials properties by simulation of the models response to load as a function of structure.

We admit that presently only experimental indications on the complexity of the mechanisms and the ranges of their activity can be reported. Nevertheless, such results appear to be an advance, compared to the predominantly homogeneous models[41] which are commonly used to predict the properties of polymers.

The results presented in this paper are based on newly developed techniques, which have been presented and compared elsewhere. Because polypropylene can show discrete small-angle scattering over a wide range of scattering angles, scattering patterns have been combined. An own article describes this technique which is based on desmearing and merging.[42] Moreover, the earlier stretch-hold technique results in distinctly different results when applied to polypropylene. The reason is a considerable relaxation of nanostructure, which starts immediately after stopping the extensometer (cf.[43] and Section 4.2.5).

2 Experimental

Material. Commercial hard-elastic[33,44] polypropylene (PP) film (CelGard-PP®, Lot #884, as extruded by Hoechst-Celanese) of 25 μm thickness is studied. The films are produced[34] from the isotactic PP grade Hercules Profax 6301 with a melt index 15.0(230°C) ASTM-D-1238. The weight-average molecular mass of the grade is $\bar{M}_w = 128000$ g/mol. The polydispersity of the material is $\bar{M}_w/\bar{M}_n = 4$. Test "bars" conforming to DIN 53504 are punched from the double-layer film resulting in samples of 50 μm thickness. For this purpose a toggle-lever press manufactured by Zwick GmbH, Ulm, Germany is used. The axis of the test bar is oriented parallel to the principal axis of the uniaxially oriented films. Fiducial marks are applied by a common rubber stamp with a line grid of 2 mm distance.

Laboratory Tensile Tests. Cross-section change of the central part of the test bar during mechanical tests is studied before the synchrotron experiments in the laboratory by a commercial extensometer (Zwicki Z1.0/TH1S, Zwick GmbH, Ulm, Germany).

SAXS Environment. SAXS is performed at the synchrotron beamline A2 at HASYLAB, Hamburg, Germany. The wavelength of the X-ray beam is 0.15 nm, and the sample-detector distance is 3045 mm. Scattering patterns are collected by a two-dimensional position sensitive marccd 165 detector (mar research, Norderstedt, Germany) operated in 2048×2048 pixel mode (pixel size: $79 \times 79\,\mu\mathrm{m}^2$).

USAXS Environment. USAXS is performed at the synchrotron beamline BW4 at HASYLAB, Hamburg, Germany. The wavelength of the X-ray beam is 0.138 nm, and the sample-detector distance is 8906 mm. Detection and registration of the scattering patterns is the same as in the SAXS environment.

Tensile Test at the Beamlines. Tensile testing at the beamlines is performed with a self-made extensometer fit for application at HASYLAB beamlines, which has been built by one of us (T.S.). The machine performs symmetric drawing. Signals from load cell and transducer are recorded during the experiment. The sample is monitored (cf. Fig. 1a) by a TV-camera, and video frames are grabbed and stored together with the experimental data. The experiment control software permits to define 8 intervals of different crosshead movement. In all experiments the machine is operated at velocities of either 2 mm/min (straining) or -2 mm/min (relaxation), respectively (cf. Fig. 1d).

The true elongation $\varepsilon = (\ell - \ell_0)/\ell_0$ is computed from the initial distance, ℓ_0, of the two fiducial marks enclosing the point of beam-irradiation, and the respective actual distance, ℓ (cf. Fig. 1a). During dynamic tensile testing between$\varepsilon = 0$ and $\varepsilon = 0.6$ the true strain rate, $\dot{\varepsilon}$, has been found to increase monotonously from $0.8 \times 10^{-3}\mathrm{s}^{-1}$ to $1.1 \times 10^{-3}\mathrm{s}^{-1}$.

Scattering patterns are recorded every 60 s with an exposure of 49 s. Progress is observed on monitors (Fig. 1) outside the experimental hutch. One of the monitors shows the TV-image of the sample with the irradiation zone of the

synchrotron beam indicated. For every SAXS pattern that is recorded, several video pictures are grabbed and stored together with the elapsed time. Other monitors display the actual SAXS pattern, the progress of the experiment reflected in the engineering stress-strain curve, and the progress of the extensometer program. Time, force and the distance of the cross-heads are continuously recorded in an ASCII file. From this file the force can directly be associated to each scattering pattern. The true elongation is manually determined after the end of the experiment. For this purpose the fiducial marks visible in the video pictures are consulted.

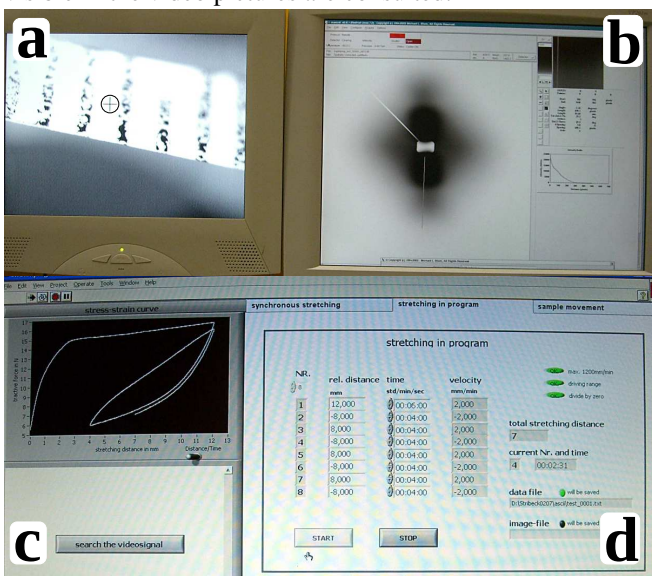

Figure 1: Mechanical testing of polypropylene in progress at HASYLAB as watched on monitors. a) Sample with fiducial marks. The area of X-ray irradiation marked by an encircled cross-hair. b) Actual SAXS pattern. c) Mechanical progress (force vs. machine strain). d) Programming window

3 Data Evaluation

3.1 Pattern Merging and Desmearing

The applied evaluation of SAXS patterns requires the recording of low-noise images over the whole angular range where discrete scattering has been observed. Because the material shows both SAXS and USAXS, the SAXS has been desmeared and merged with the USAXS pattern as described in a previous article.[42]

3.2 Chord-Distribution Function Analysis

Our analysis starts from the scattering pattern and turns it into a representation of the nanostructure in real space. The only assumption is presence of a multiphase topology. The result is a multidimensional chord distribution function (CDF), $z(\mathbf{r})$.[32] The method is exemplified in a textbook (Stribeck,[30] Sect. 8.5.5). For a schematic sketch of the steps of data analysis and the extraction of structural parameters from the CDF see for example Fig. 2 in Stribeck et al.[45] The method is extracting the topological information on nanostructure (e.g. a two-phase topology, $\rho(\mathbf{r}) \in \left[\rho_{\text{cryst}}, \rho_{\text{amorph}}\right]$, of phases with distinct densities) from two-dimensional (2D) SAXS patterns with uniaxial symmetry. The resulting CDF is an "edge-enhanced autocorrelation function"[46–49] – the autocorrelation of the gradient field, $\nabla\rho(\mathbf{r})$. Thus, as a function of ghost displacement, $\mathbf{r}$, the multidimensional CDF $z(\mathbf{r})$ shows peaks wherever there are *domain surface contacts* between domains in $\rho(\mathbf{r})$ and in its displaced ghost. The CDF with fiber symmetry in real space, $z(r_{12}, r_3)$, is computed from the fiber-symmetrical SAXS pattern, $I(s_{12}, s_3)$, of multi-phase materials.[32] $\mathbf{s} = (s_{12}, s_3)$ is the scattering vector with its modulus defined by $|\mathbf{s}| = s = (2/\lambda)\sin\theta$. Here λ is the wavelength of radiation, and 2θ is the scattering angle. In the historical context the CDF is an extension of Ruland's interface distribution function (IDF)[50] to the multidimensional case or, in a different view, the Laplacian of Vonk's multidimensional correlation function.[51]

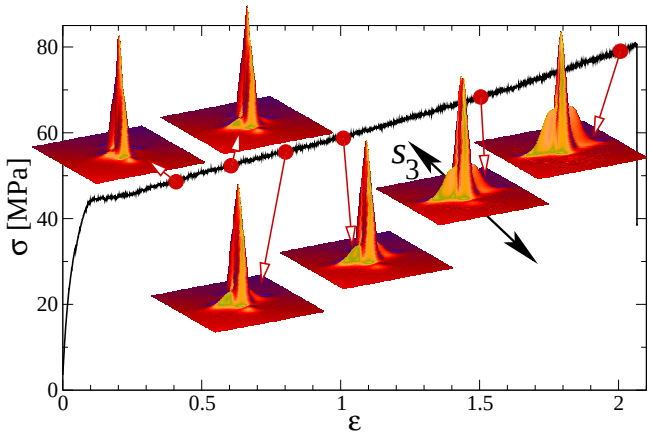

Figure 2: Hard-elastic Polypropylene. Continuous straining until break monitored by SAXS. The SAXS patterns show a region -0.17 $\text{nm}^{-1} < s_{12,}s_3 <$0.17 nm^{-1}. The black arrow in one of the SAXS patterns indicates the straining direction (s_3). Intensity on a logarithmic scale

4 Results and Discussion

4.1 Straining until Break

In the classical mechanical test the material has been extended until rupture. As the test is continuously monitored by SAXS (Fig. 2), no remarkable changes are found in the long linear part of the stress-strain curve. With increasing elongation, the higher orders of the long period are vanishing. All in all, the scattering of the material is strongly decreasing (in the leftmost pattern the intensity is 10fold the intensity of the rightmost pattern). During the test the relative strength of an equatorial streak is increasing. If the patterns are interpreted directly, the growth of the distance between neighboring crystalline lamellae (long period) can be compared to the macroscopic elongation. The practical value of such results for the

understanding of the nanomechanics is considered limited.[31]

Considerable changes which appear interesting for application are observed in the interval of low elongations ($0 < \varepsilon < 0.4$), which is again observed in the load-cycling experiment. The corresponding results are presented in the respective Section 4.2.

Moreover, the data of the continuous-strain experiment enable us to study the nanostructure evolution of hard-elastic polypropylene in the vicinity of rupture under dynamical conditions for the first time as compared to the stretch-hold technique.[6,43] As already shown by the scattering patterns (Fig. 2), the scattering of the ensemble made from crystalline and amorphous lamellae is continuously decreasing while the equatorial scattering of a fibrillar system becomes more obvious. Whether or not there are still uncorrelated lamellae present at break, is difficult to tell from the scattering patterns directly. Therefore we compute the multidimensional chord-distribution function (CDF)[32] and monitor the nanostructure evolution in physical space. Figure 3 shows the result. Already at an elongation $\varepsilon = 1$ the influence of the nascent equatorial streak from the SAXS pattern is present in the CDF. Across the strong layer reflections two sharp ridges are running in the direction parallel to the meridian (r_3). They show the presence of needle-shaped domains.[52,53] Only two ridges are visible. Thus, the distances among neighboring needles are not correlated. At $\varepsilon = 1$ the layers are still predominant. The width of the respective reflections (label: "le") is related to their lateral extension.

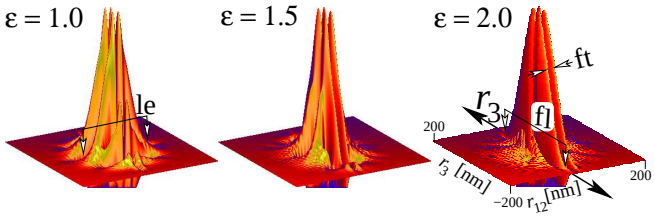

Figure 3: Hard-elastic Polypropylene. CDFs $z(r_{12}, r_3)$ on a logarithmic scale as computed from SAXS data taken during a continuous straining experiment with an elongation at break, $\varepsilon_b = 2.1$. At $\varepsilon = 1$ a layer system is observed. The length labeled "le" indicates double the average extension of the layers. At $\varepsilon = 2$ the layer system is just vanishing. Labels "fl" and "ft" indicate average length and thickness of the remnant needle-shaped domains, respectively

At $\varepsilon = 1.5$ the lamellae system is no longer prevailing. At $\varepsilon = 2.0$ the last layers are vanishing. The nanostructure is made from uncorrelated needles. Thus, the material disrupts when all the lamellae have been consumed. The same result is reported from straining experiments of polyamide-6.[54]

Moreover, it appears noteworthy that the average thickness of the needles is constant (8 nm) during the experiment. This value is considerably higher than the experimental resolution ($1/s_{max}$ with $s_{max} = 0.18$ nm^{-1}) of the SAXS setup. Therefore we assume that this finding is no artifact, but an indication of a nanostructural feature. Because the needles do not exhibit transverse contraction, they should consist of rigid material. Such needles may be identified by the fibrillar crystallites as described by Noether.[33]

4.2 Load-Cycling

In the load-reversal experiment the elongation of the sample is oscillated in the elastic[33] regime of the hard-elastic material.

4.2.1 The First-Cycle Scattering Patterns

The lapse of the stress-strain curve and some of the recorded and combined SAXS/USAXS patterns are shown in Fig. 4.

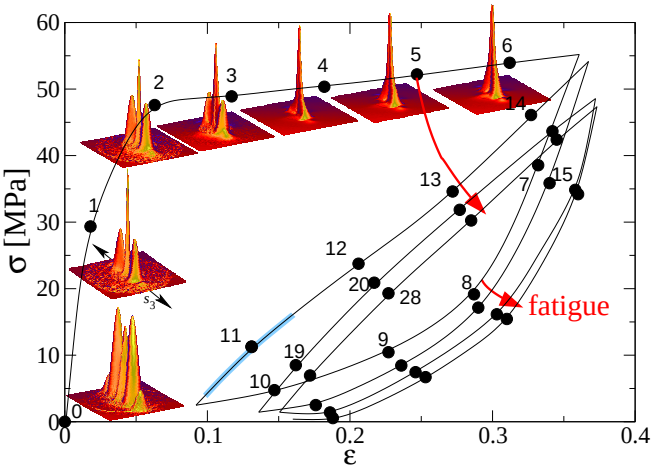

Figure 4: Hard-elastic Polypropylene. Load-reversal mechanical test monitored by SAXS. Circular dots show where SAXS patterns have been recorded. Numerical labels indicate their sequence. The highlighted part of the curve near label 11 indicates the part of the curve traversed during the recording of pattern 11. The drawing direction with respect to the patterns, s_3, is indicated by a double-head arrow. The scattering patterns display the range -0.15 nm^{-1} $< s_{12}, s_3 <$0.15 nm^{-1}

Filled circles on the curve mark the average elongations and stresses related to the recorded scattering patterns. Numbers placed beside some of the circles indicate the serial number of the respective pattern. While a single pattern is exposed, stress and strain are continuously changing. The highlighted part of the curve around pattern 11 indicates the region that has been traversed during its exposure.

In Fig. 4 the first 7 scattering patterns are strung alongside the stress-strain curve. The unstrained material (pattern 0) exhibits on the meridian (s_3) the typical two-point diagram of a highly oriented lamellae ensemble. Even a strong 2nd order of the long period peak is visible. The central scattering and the USAXS is moderate. Just after the beginning of the test (pattern 1) the USAXS in the center has considerably increased. The graphics had to be re-scaled, and therefore the 1st-order long-period peak looks weaker. In fact, only the 2nd-order peaks have become weaker. The reflections appear blurred up to the beginning of the long linear region of the curve. The scattering patterns are continuously changing,

and exhibit several overlapping features. Thus, it appears inappropriate to directly interpret the patterns resorting to simplified structural notions.

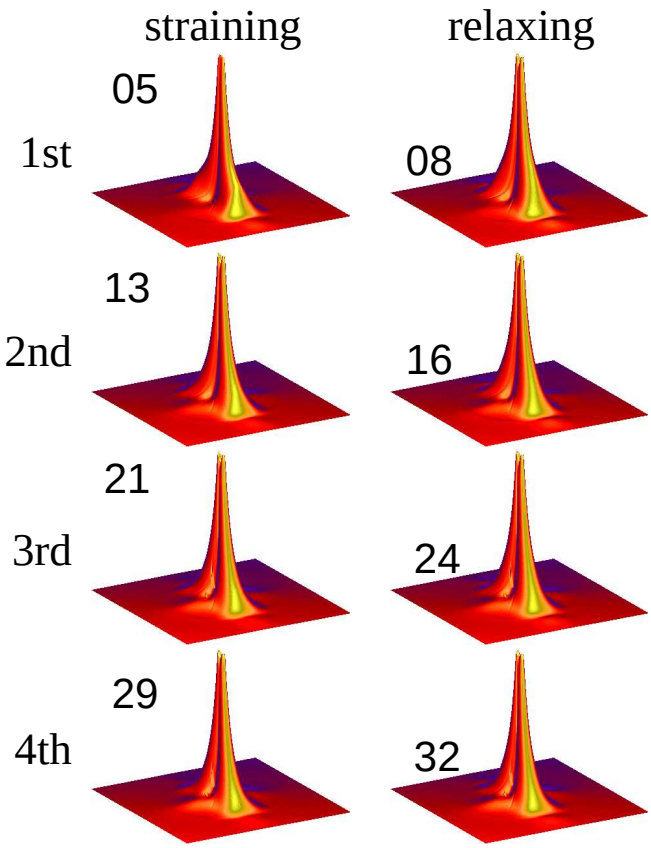

Figure 5: Load-reversal test of polypropylene monitored by SAXS. Variation of the scattering pattern at constant machine elongation (cf. Fig. 4, label "fatigue") in 4 cycles under strain (left) and during relaxation (right), respectively. The patterns show the combined SAXS/USAXS intensity in the region -0.1 $nm^{-1} < s_{12}, s_3 <$0.1 nm^{-1}. Numerical labels indicate the serial number of scattering patterns

4.2.2 Fatigue: Variation of Scattering from Cycle to Cycle

Mechanical fatigue of the material can be studied by following the curved arrows in Fig. 4. The corresponding scattering patterns are shown in Fig. 5. Again, direct interpretation of observed features does not return quantitative information on the evolution of the nanostructure made from crystalline and amorphous domains. The long-period peaks are too wide for a thorough determination of their position. Information on the lateral extension of the lamellae is hardly accessible. An exception is the scattering power that exhibits considerable oscillations. Therefore the presentation shows patterns which are normalized to their highest intensity. For a quantitative analysis one may now try to extract the topological information of the two-phase structure from the scattering patterns, and to display it in real space as a CDF.[32]

4.2.3 First Cycle: CDF Analysis

The first 4 patterns recorded monitor the steep linear increase of the stress-strain curve (cf. Fig. 4, patterns 0-3). The corresponding multidimensional chord-distribution functions[30,32] are presented in Fig. 6.

The experiment has been reproduced 3 times with different samples. The unstrained material shows the typical CDF of a highly oriented ensemble of layers. Counted from the center, 4 peaks of nearly triangular shape and decreasing height are observed. These peaks are generated at positions, which correspond to the average distances of layer surfaces from each other. Compared to other technical polymer materials, the range of order between the crystalline lamellae is quite high. The width of the broadest triangles in the direction of r_{12} is related to the lateral extension of the lamellae. The distance between neighboring lamellae from each other is the long period L. An average value is given by the position of the first minimum of the CDF on the meridian, r_3 (cf. Fig. 8). For the unstrained material we determine L =17.7 nm.

At ε =0.02 we still find the same long period (L =17.8 nm). We now discover only 3 correlated layers in the stack. Noteworthy is the clear striation of the layer peaks, which is still present at ε =0.06 (L =18.8 nm). At ε =0.12 (L =20.1 nm) the yield point has been crossed, and the layer peaks are no longer striated.

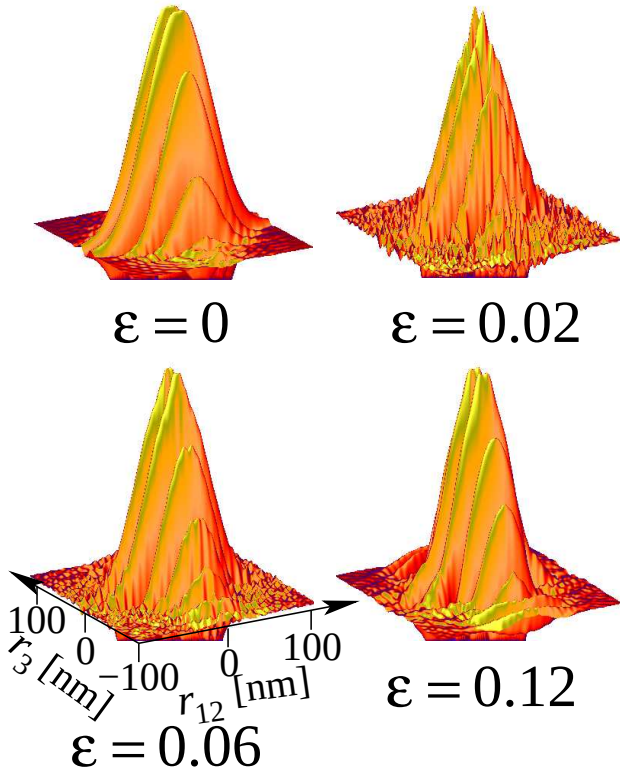

Figure 6: Chord-distribution functions $z(r_{12}, r_3)$ on a logarithmic intensity scale showing the nanostructure evolution in highly oriented polypropylene as a function of true elongation, ε. Combined SAXS/USAXS data recorded in time-resolved dynamic straining experiments

Such a striation means that at least some of the layers must have been subjected to a density modulation in lateral direction. This modulation can either be attributed to the amorphous, or to the crystalline layers. Thus, either nanometer-size voids are torn open in some amorphous layers, or some of the crystalline layers are breaking into blocks. Moreover, because after the yield point there are only smooth lamellae left over, the nanopores must have been merged into micropores, or the fragments of the weak lamellae must have molten. Figure 7 sketches the two possibilities. The generation of microporosity[38,39,44] in hard-elastic thermoplastic material by straining is the basis of an important technical application of these polymers. Nevertheless, according to experience microporosity is only created, if the straining direction and the orientation direction of the material are different.[40]

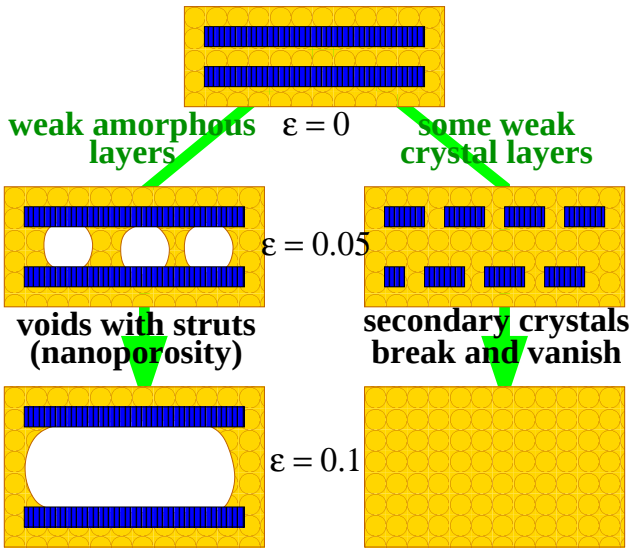

Figure 7: Two possible topological models for the explanation of the "blocky layers" observed in the scattering data of hard-elastic polypropylene during straining

If the observed dissection of lamellae peaks is a result of nanoporosity (left path in Fig. 7), the integral $S = \int z(r_{12}, r_3)\, dr_{12} dr_3$ must increase considerably, because it is proportional to the inner surface of the nanostructure multiplied by the square of the density jump at the phase boundary. This density jump becomes extreme upon formation of voids.

On the other hand, if the dissection is attributed to the failure of weak lamellae directly followed by melting of the fragments (right path in Fig. 7), the disappearance is reducing the surface, and the strength S of the CDF signal has to decrease.

Not only the strength S, but also some other nanostructure parameters can easily be extracted from the CDF. The applied procedures are sketched in Fig. 8. The average long period, L, is determined from the position of the minimum between the first and the second triangular peak. Half the base-length of the second triangular peak is a measure of the lateral extension, e_{cac}, of a sandwich made from two layers of one kind which are separated by one layer of the other kind. Because we observe that the correlation among layers is low during load-cycling, e_{cac} is, to a first approximation, the lateral extension of a sandwich made from 2 crystal lamellae. We have chosen this measure instead of measuring the extension of a single crystalline layer, because this feature is strongly interfering with a peak that indicates the formation of bridges between neighboring layers (cross-hatched structure[55]). Therefore a determination requires peak separation, whereas e_{cac} can be determined graphically. The phenomenon of bridge formation has been reported in a previous study on the nanostructure relaxation after stopping the extensometer.[43]

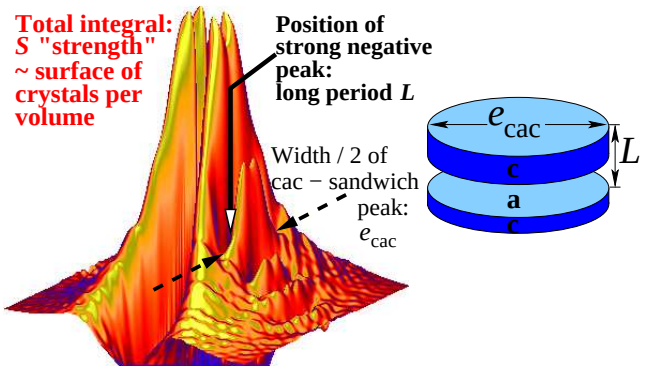

Figure 8: Simple methods of nanostructure parameter extraction from a CDF. The strength S is a measure of surface between crystals and amorphous layers, L is an average long period, and e_{cac} is an average lateral extension of the layer-shaped domains

The strength is $S(\varepsilon = 0)$ =30 (in relative units) for the unstrained material. With increasing elongation it is initially decreasing ($S(\varepsilon = 0.02)$ =15, $S(\varepsilon = 0.06)$ =5), and begins to increase, again, after the yield point has been reached ($S(\varepsilon = 0.12)$ =11, $S(\varepsilon = 0.18)$ =28). From pattern 0 to pattern 4 the long period L is continuously increasing ($L(\varepsilon = 0)$=18 nm, $L(\varepsilon = 0.18)$=23 nm), but the lateral extension shows no increase ($e_{cac}(\varepsilon = 0)$ =30 nm, $e_{cac}(\varepsilon = 0.18)$ =25 nm). In particular the decrease of S only permits to conclude that the initial striation of the layer reflections in the CDF is related to a breakup of some (e.g. weak, secondary) crystal lamellae. Thus, the time-resolved experiment shows that the weak lamellae do not melt down from their borders, but disrupt into a mesostructure of blocks first, before they vanish. Moreover, the observed long-ranging striation shows that the blocks are arranged rather regularly in the plane of their "mother layer" – similar to the pieces in a chocolate bar. This blocky mesostructure of polypropylene has first been found and described by Strobl[56] in crystallization experiments of polypropylene. Now our experiments indicate that even during mechanical loading of weak polypropylene lamellae, this mesostate may be traversed. In conjunction with the notions developed for crystallization of lamellae from blocks, it appears suggesting that poorly welded lamellae are breaking into their constituents before the latter are melting. Moreover, such blocks have even been observed in an electron microscopic study of pre-stretched hard-elastic material (,[40] Fig. 10a), when the direction of

strain is the orientation direction of the material. However, the material studied is not polypropylene but polyethylene. In excess of the results of electron microscopy, our in situ scattering experiment exhibits that (1) already at low elongation blocks are generated by breaking lamellae, (2) the pieces are placed at regular intervals, (3) the pieces are dynamically torn apart and vanish (melt). This observation of early block melting is in full agreement with the results of a deformation calorimeter study[57] of hard-elastic polypropylene. The authors report a clear partial melting effect for $0 < \varepsilon < 0.1$. According to the study, the melting effect is considerably reduced, if the material has been annealed at high temperature before straining. From the wavelength of lateral undulation on the layer peaks, we estimate an average distance between the blocks of 10 nm for $\varepsilon = 0.02$. At $\varepsilon = 0.12$ the amplitude of the undulation is much lower, and the wavelength of block arrangement has grown to 25 nm.

4.2.4 Fatigue: CDF and Nanostructure Evolution from Cycle to Cycle

In order to discuss the evolution, we have plotted the resulting nanostructure parameters together with the macroscopic mechanical data as a function of the elapsed time t. Figure 9 presents the result.

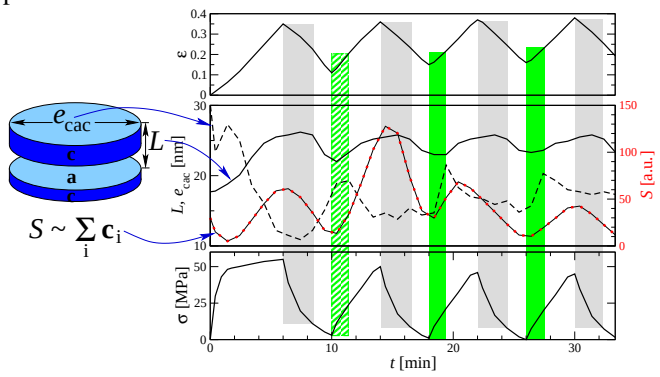

Figure 9: Dynamic load-reversal mechanical test of hard-elastic PP film at a strain rate of $\dot{\varepsilon} \approx 10^{-3}\mathrm{s}^{-1}$. As a function of the elapsed time t the macroscopic parameters elongation, ε (top graph), and tensile stress, σ (bottom graph) are displayed together with topological nanostructure parameters (middle). In the middle diagram the solid line shows the long period, L. The broken line displays the lateral extension, e_{cac}, of a sandwich made from two crystalline lamellae. The line with circular dots exhibits the variation of the strength, S, of the CDF. Vertical bars indicate zones of strain-induced crystallization (dark green) and relaxation-induced melting (light gray), respectively

The top chart shows the true elongation, $\varepsilon(t)$, imposed to the material and measured at the point of X-ray irradiation. The four load-reversal cycles are easily identified. The chart in the middle reports the extracted nanostructure parameters, $L(t)$, $e_{cac}(t)$, and $S(t)$. The bottom diagram presents the macroscopic resistance, $\sigma(t)$, which the material is opposing to strain.

First, let us examine the regions in each strain cycle that are highlighted in light-gray and start at the top dead center. During each of these intervals the long period, L, is almost constant on a high level. Simultaneously, in each cycle, $S(t)$, (crystallite surface, i.e. approximately the number of lamellae) is considerably decreasing, whereas the lateral extension of the layers is hardly changing. Altogether, this observation appears to be an indication for relaxation melting of crystalline lamellae. To the right of the light-gray boxes but still before the end of the relaxation half-cycle, the long period is considerably decreasing, whereas the decrease of S is slowing down. Now the melting process is no longer predominant, and the contraction of the amorphous phase is reflected in the decrease of the average long period.

During the entire 2nd straining phase $S(t)$ is increasing. Nevertheless, the process does not appear to be a simple one: In the beginning the lateral extension of the lamellae remains high. This finding may be explained by moderate strain-induced crystallization (highlighted by a hatched dark-green box). To the right of this box the lateral extension e_{cac} is decreasing. A possible explanation is a generation of surface S by rupture of crystalline lamellae into stable fragments. The lateral extension of the fragments is low (15 nm) at an average long period of 25 nm.

Let us now discuss the regions indicated by filled dark-green boxes in the 3rd and the 4th cycle. They are extending from the bottom dead center into the region of straining and end where the stress exceeds* $\sigma(t) > 20$ MPa. In spite of the continuous straining, the long period remains on a low level, whereas the lateral extension of the crystallites is strongly increasing. An increase of S is observed, as well. This is a clear indication of strain crystallization. If existing crystallite blocks would simply merge, the long period would have to increase and S would decrease or stay constant.

However, the crystallization is not continued throughout the entire ascent of strain. After the end of the intervals marked in dark-green, the average lateral extension of the lamellae is suddenly decreasing. This observation can be explained by disruption of extended lamellae due to the applied high stress. The increasing long period supports the interpretation that crystallization has considerably slowed down. Thus, it appears convincing that in the middle of the straining branch a new nanostructure evolution mechanism is setting in, namely crystal disruption. The identification of such points in the load cycle appears to be important both for an understanding of the mechanical properties and for the design of models which are capable to predict mechanical properties of complex polymer materials.

Finally, we turn to the structure variation in the first straining cycle between 2 min$< t <$6 min (ε: 0.1→0.35), in which the stress, $\sigma(t)$, is only moderately increasing. Here we observe a linear increase of S, accompanied by increasing long

*In a book chapter[58] some of the data have been presented in order to demonstrate the method. All the stress values given there are by 27 MPa too high, because we had forgotten to subtract the basic load imposed by the weight of the upper cross-head.

period and decreasing lateral extension of the crystallites. This finding may be interpreted as an indication for a superposition of strain crystallization and disruption of extended lamellae.

In summary, it appears most probable that crystallization, rupture of lamellae and melting of fragments are continuously reshaping the domains of the polypropylene material in the repeated cycles of a fatigue test. The long-period cycle exhibits a phase shift with respect to the imposed strain cycling. Moreover, there is an indication of amplitude attenuation. The curve $\sigma(t)$ is demonstrating the fatigue of the material by decreasing stress peaks.

4.2.5 Structure Relaxation after the Load-Reversal Test

As reported in a previous paper,[43] the nanostructure information gathered by SAXS is different for polypropylene, if the SAXS pattern is exposed while the extensometer is idle. Let us demonstrate the effect by investigating what happens after the load-cycle test is finished. Directly after the machine has been stopped, an additional scattering pattern has been recorded. The comparison is shown in pseudo-color in Fig. 10. On the left side of the figure, i.e. while the machine has still been running, the CDF exhibits smooth streaks of an ensemble of extended lamellae. On the right, i.e. during the first minute after machine stop, the CDF additionally shows blocky domains. Moreover, the blocks appear arranged in the lateral plane. This is indicated by the regular modulation of the central streak. The finding can be explained by block crystallization which sets in as the extensometer is stopped.

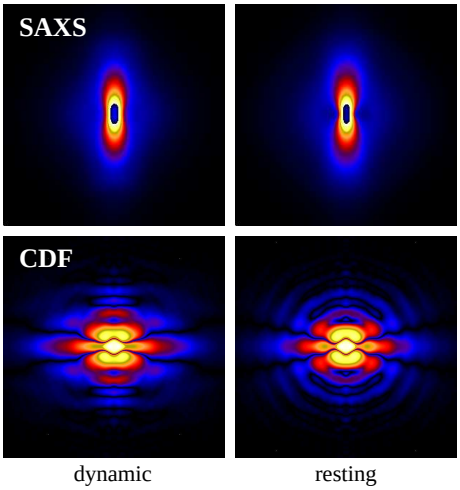

Figure 10: Nanostructure relaxation during the first minute of rest after the load-cycling experiment at $\varepsilon = 0.18$ on logarithmic scales. The SAXS patterns in the top represent a square of -0.08 nm^{-1}< s_{12}, s_3 <0.08 nm^{-1} in identical scaling. The central dark spot is a result of intensity overflow. The bottom row shows $|z(r_{12}, r_3)|$ (-100 nm< r_{12}, r_3 <100 nm). Straining direction (s_3 and r_3, resp.) is vertical

4.2.6 Mechanisms in the stress-strain diagram

A sketch in which the discussed mechanisms are projected onto the stress-strain diagram of the load-cycle experiment is presented in Fig. 11.

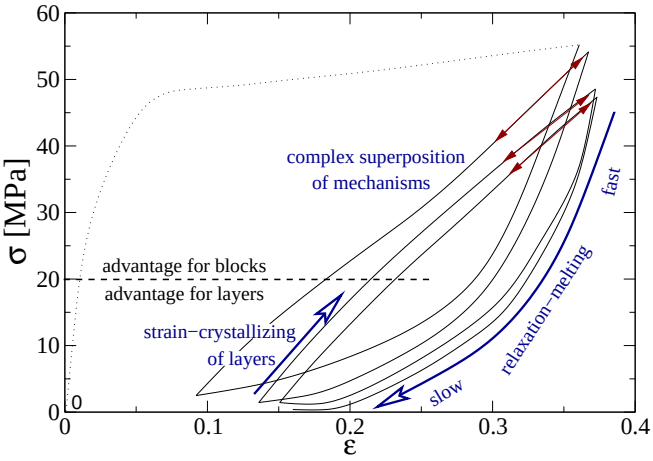

Figure 11: Mechanisms of nanostructure evolution in the stress-strain diagram of a slow load-cycling test of hard-elastic polypropylene

For the relaxation branches of all the cycles our SAXS analysis is indicating the same kind of mechanism. Relaxation triggers the melting of crystalline domains, and this process is slowed down as the branch is traversed.

In the beginning of the strain branches it appears just the opposite: strain crystallization is widening existing lamellae and introducing new ones. As a limiting stress of 20 MPa is exceeded, the slope of the strain branches becomes somewhat less steep and lamellae disruption is starting. Nevertheless, in the 2nd and 4th cycle the SAXS analysis tells that strain crystallization (now of blocky crystallites) remains dominant, whereas a lot of weak blocks appear to be molten in the 3rd cycle. This is a strange observation and shows the limits of our analysis, although there is an indication in the stress-strain curve itself that is supporting our strange finding. Namely, the final slope of the strain branch (arrows with triangular filled double head) is less steep in the 3rd cycle. Thus, as the SAXS analysis yields an indication that melting of weak blocks is predominant, the material appears to be softer than in those cases where crystallization of new blocks appears to dominate.

5 Conclusion

In our study we have tested the possibility to monitor the evolution of nanostructure in a semicrystalline polymer material during a mechanical test by X-ray scattering. With some effort and for low strain rates this is already possible using presently available instrumentation. The experiment yields a description of the dynamic mechanisms, which are responsible for rupture or fatigue of the material.

Soon the time-resolution will become much better, when

detectors based on the PILATUS principle[59] will be available. Even the number of powerful synchrotron sources will soon be increasing. Then it will become possible to substantially increase the strain rate without loosing image quality, and, thus, to approach strain rates in the range of practical relevance.

Acknowledgment. We acknowledge HASYLAB, Hamburg, for provision of the synchrotron radiation facilities at beamlines A2 and BW4. Financial support by the European Commission under the 7th Framework Programme in the project NANOTOUGH is gratefully acknowledged.

References

[1] D. J. Hughes, A. Mahendrasingam, C. Martin, W. B. Oatway, E. L. Heeley, S. J. Bingham, W. Fuller, *Rev. Sci. Instrum.* **1999**, *70*, 4051.
[2] M. F. Butler, A. M. Donald, W. Bras, G. R. Mant, G. E. Derbyshire, A. J. Ryan, *Macromolecules* **1995**, *28*, 6383.
[3] M. F. Butler, A. M. Donald, A. J. Ryan, *Polymer* **1997**, *38*, 5521.
[4] D. J. Hughes, A. Mahendrasingam, W. B. Oatway, E. L. Heeley, C. Martin, W. Fuller, *Polymer* **1997**, *38*, 6427.
[5] D. J. Blundell, A. Mahendrasingam, D. McKerron, A. Turner, R. Rule, R. J. Oldman, W. Fuller, *Polymer* **1994**, *35*, 3875.
[6] J. Wu, J. M. Schultz, F. Yeh, B. S. Hsiao, B. Chu, *Macromolecules* **2000**, *33*, 1765.
[7] M. Brandt, W. Ruland, *Acta Polym.* **1996**, *47*, 498.
[8] L.-Z. Liu, B. S. Hsiao, B. X. Fu, S. Ran, S. Toki, B. Chu, A. H. Tsou, P. K. Agarwal, *Macromolecules* **2003**, *36*, 1920.
[9] W. Wilke, M. Bratrich, *J. Appl. Cryst.* **1991**, *24*, 645.
[10] D. Grubb, V. Bala, *Polym. Mater. Sci. Eng.* **1999**, *81*, 357.
[11] B. X. Fu, B. S. Hsiao, S. Pagola, P. Stephens, H. White, M. Rafailovich, J. Sokolov, P. T. Mather, H. G. Jeon, S. Phillips, J. Lichtenhan, J. Schwab, *Polymer* **2000**, *42*, 599.
[12] F. Yeh, B. S. Hsiao, B. B. Sauer, S. Michel, H. W. Siesler, *Macromolecules* **2003**, *36*, 1940.
[13] N. Stribeck, S. Polizzi, P. Bösecke, H. G. Zachmann, *Rev. Roumaine Chem.* **1989**, *34*, 635.
[14] N. Stribeck, P. Bösecke, S. Polizzi, *Colloid Polym. Sci.* **1989**, *267*, 687.
[15] N. Stribeck, *J. Polym. Sci., Part B: Polym. Phys.* **1999**, *37*, 975.
[16] N. Stribeck, S. Fakirov, D. Sapoundjieva, *Macromolecules* **1999**, *32*, 3368.
[17] S. Fakirov, O. Samokovlijsky, N. Stribeck, A. A. Apostolov, Z. Denchev, D. Sapoundjieva, M. Evstatiev, A. Meyer, M. Stamm, *Macromolecules* **2001**, *34*, 3314.
[18] N. Stribeck, E. Buzdugan, P. Ghioca, S. Serban, R. Gehrke, *Macromol. Chem. Phys.* **2002**, *203*, 636.
[19] N. Stribeck, R. Androsch, S. S. Funari, *Macromol. Chem. Phys.* **2003**, *204*, 1202.
[20] N. Stribeck, S. Fakirov, A. A. Apostolov, Z. Denchev, R. Gehrke, *Macromol. Chem. Phys.* **2003**, *204*, 1000.
[21] N. Stribeck, S. S. Funari, *J. Polym. Sci. Part B: Polym. Phys.* **2003**, *41*, 1947.
[22] B. B. Sauer, R. S. McLean, D. J. Brill, D. J. Londono, *J. Polym. Sci. Part B: Polym. Phys.* **2002**, *40*, 1727.
[23] S. Murakami, M. Yamakawa, M. Tsuji, S. Kohjiya, *Polymer* **1996**, *37*, 3945.
[24] R. Séguéla, J. Prud'homme, *Macromolecules* **1988**, *21*, 635.
[25] H. S. Lee, S. R. Yoo, S. W. Seo, *J. Polym. Sci., Part B: Polym. Phys.* **1999**, *37*, 3233.
[26] G. E. Welsh, D. J. Blundell, A. H. Windle, *J. Mater. Sci.* **2000**, *35*, 5225.
[27] J. J. Hernández, M. C. García Gutiérrez, A. Nogales, D. R. Rueda, A. Sanz, I. Sics, B. S. Hsiao, Z. Roslaniec, G. Broza, T. A. Ezquerra, *Polymer* **2007**, *48*, 3286.
[28] X. Chen, K. Yoon, C. Burger, I. Sics, D. Fang, B. S. Hsiao, B. Chu, *Macromolecules* **2005**, *38*, 3883.
[29] D. J. Blundell, G. Eeckhaut, W. Fuller, A. Mahendrasingam, C. Martin, *J. Macromol. Sci. Phys.* **2004**, *43*, 125.
[30] N. Stribeck, *X-Ray Scattering of Soft Matter*, Springer, Heidelberg, New York, **2007**.
[31] P. Debye, H. Menke, *Erg. techn. Röntgenkunde* **1931**, *2*, 1.
[32] N. Stribeck, *J. Appl. Cryst.* **2001**, *34*, 496.
[33] H. D. Noether, *Intern. J. Polymeric Mater.* **1979**, *7*, 57.
[34] H. D. Noether, W. Whitney, *Colloid Polym. Sci.* **1973**, *251*, 991.
[35] I. K. Park, H. D. Noether, *Colloid Polym. Sci.* **1975**, *253*, 824.
[36] S. Hild, W. Gutmannsbauer, R. Luthi, J. Fuhrmann, H.-J. Guntherodt, *J. Polym. Sci. Part B Polym. Phys.* **1996**, *34*, 1953.
[37] J. Xu, M. Johnson, G. L. Wilkes, *Polymer* **2004**, *45*, 5327.
[38] M. B. Johnson, G. L. Wilkes, *J. Appl. Polym. Sci.* **2002**, *83*, 2095.
[39] M. B. Johnson, G. L. Wilkes, *J. Appl. Polym. Sci.* **2001**, *81*, 2944.
[40] G. L. Wilkes, H. Zhou, *J. Mater. Sci.* **1998**, *33*, 287.
[41] J. Bicerano, *Prediction of Polymer Properties*, CRC Press, New York, 3rd edition, **2002**.
[42] N. Stribeck, U. Nöchel, *J. Appl. Cryst.* **2008**, , accepted.
[43] N. Stribeck, U. Nöchel, S. S. Funari, T. Schubert, *J. Polym. Sci. Polym. Phys.* **2008**, *46*, 721.
[44] B. S. Sprague, *J. Macromol. Sci. Phys.* **1973**, *B8*, 157.
[45] N. Stribeck, A. Almendarez Camarillo, U. Nöchel, C. Schroer, M. Kuhlmann, S. V. Roth, R. Gehrke, R. K. Bayer, *Macromol. Chem. Phys.* **2006**, *207*, 1239.
[46] P. Debye, A. M. Bueche, *J. Appl. Phys.* **1949**, *20*, 518.

[47] G. Porod, *Colloid Polym. Sci.* **1951**, *124*, 83.
[48] C. G. Vonk, *J. Appl. Cryst.* **1973**, *6*, 81.
[49] F. J. Baltá Calleja, C. G. Vonk, *X-Ray Scattering of Synthetic Polymers*, Elsevier, Amsterdam, **1989**.
[50] W. Ruland, *Colloid Polym. Sci.* **1977**, *255*, 417.
[51] C. G. Vonk, *Colloid Polym. Sci.* **1979**, *257*, 1021.
[52] G. Porod, *Fortschr. Hochpolym.-Forsch.* **1961**, *2*, 363.
[53] W. O. Statton, *Z. Kristallogr.* **1968**, *127*, 229.
[54] N. S. Murthy, D. T. Grubb, *J. Polym. Sci. Part B: Polym. Phys.* **2002**, *40*, 691.
[55] D. R. Norton, A. Keller, *Polymer* **1985**, *26*, 704.
[56] T. Hugel, G. Strobl, R. Thomann, *Acta Polym.* **1999**, *50*, 214.
[57] D. Göritz, F. H. Müller, *Colloid Polym. Sci.* **1974**, *252*, 862.
[58] N. Stribeck, in: J. Karger-Kocsis, S. Fakirov, Eds. "Nano- and Micromechanics of Polymer Blends and Composites", Hanser Publisher, München, vol. 1, **2008** pp. x–xx.
[59] C. Broennimann, E. F. Eikenberry, B. Henrich, R. Horrisberger, G. Hülsen, E. Pohl, B. Schmitt, C. Schulze-Briese, M. Suzuki, T. Tomizaki, A. Toyokawa, A. Wagner, *J. Synchrotron Rad.* **2006**, *13*, 120.

Synopsis. Time-resolved X-ray scattering of poly(propylene) during mechanical tests reveals complex mechanisms with respect to the semicrystalline nanostructure. Crystallization, rupture of lamellae, and melting of fragments are continuously reshaping the domains of the material.